J|A|C|S
ARTICLES
Published on Web 01/13/2006

Aerosol Assisted Chemical Vapor Deposition Using Nanoparticle Precursors: A Route to Nanocomposite Thin Films

Robert G. Palgrave and Ivan P. Parkin*

Contribution from the Department of Chemistry, University College London, 20 Gordon Street, London, WC1H 0AJ, United Kingdom

Received August 26, 2005; E-mail: i.p.parkin@ucl.ac.uk

Abstract: Gold nanoparticle and gold/semiconductor nanocomposite thin films have been deposited using aerosol assisted chemical vapor deposition (CVD). A preformed gold colloid in toluene was used as a precursor to deposit gold films onto silica glass. These nanoparticle films showed the characteristic plasmon absorption of Au nanoparticles at 537 nm, and scanning electron microscopic (SEM) imaging confirmed the presence of individual gold particles. Nanocomposite films were deposited from the colloid concurrently with conventional CVD precursors. A film of gold particles in a host tungsten oxide matrix resulted from co-deposition with $[W(OPh)_6]$, while gold particles in a host titania matrix resulted from co-deposition with $[Ti(O^iPr)_4]$. The density of Au nanoparticles within the film could be varied by changing the Au colloid concentration in the original precursor solution. Titania/gold composite films were intensely colored and showed dichromism: blue in transmitted light and red in reflected light. They showed metal-like reflection spectra and plasmon absorption. X-ray photoelectron spectroscopy and energy-dispersive X-ray analysis confirmed the presence of metallic gold, and SEM imaging showed individual Au nanoparticles embedded in the films. X-ray diffraction detected crystalline gold in the composite films. This CVD technique can be readily extended to produce other nanocomposite films by varying the colloids and precursors used, and it offers a rapid, convenient route to nanoparticle and nanocomposite thin films.

Introduction

Nanoparticles are a major research focus worldwide, and a variety of different shapes and compositions can now be produced.[1,2] Many technological applications of these particles will depend on their incorporation into a host matrix; the result is a nanocomposite, which serves both to immobilize the particles and to render them chemically inert. In addition, the incorporation of nanoparticles into a matrix can change the properties of both the particle and the host. A popular topic for investigation is semiconductor/metal nanocomposites, especially noble metal nanoparticles incorporated into a semiconductor matrix.[3−10] The presence of nanoparticles can alter the Fermi level of the semiconducting host material and assist in photogenerated charge separation, and this has been exploited in improved photocatalysts,[3,11,12] photoanodes,[13] and photochromic and electrochromic films.[14,15]

Several strategies for the production of semiconductor/metal composites have been developed. As shown in Scheme 1, they can be broadly divided into four categories:

Route 1 is the synthesis of the semiconductor matrix followed by addition of preformed nanoparticles in a second step. Examples of this strategy include spin coating or dip coating a semiconductor film with a nanoparticle solution.[3,14−16] The nanoparticles are chemically bound to the surface or become trapped within pores in the semiconductor.

Route 2 is the synthesis of the semiconductor matrix followed by application of metal ions in a second step, leading to formation of metal particles in situ, within the film. High energy ion implantation[6,17,18] and spin coating with a solution of metal ions followed by photocatalytic reduction or heat treatment[8,19] are examples of this strategy.

Route 3 is the synthesis of the semiconductor matrix and metal particles in a single step. Examples include sol−gel using

(1) The Royal Society and The Royal Academy of Engineering. *Nanoscience and Nanotechnologies*; The Royal Society of Chemistry: London, 2004.
(2) *Nanoparticles*—from theory to applications; Schmid, G., Ed.; Wiley: New York, 2004.
(3) Subramanian, V.; Wolf, E. E.; Kamat, P. V. *J. Am. Chem. Soc.* **2004**, *126*, 4943.
(4) Ung, T.; Liz-Marzan, L. M.; Mulvaney, P. *Colloids Surf., A: Physicochem. Eng. Aspects* **2002**, *202*, 119.
(5) Xu, X.; Stevens, M.; Cortie, M. B. *Chem. Mater.* **2004**, *16*, 2259.
(6) Liu, Z.; Wang, H.; Li, H.; Wang, X. *Appl. Phys. Lett.* **1998**, *72*, 1823.
(7) Mokari, T.; Sertchook, H.; Aharoni, A.; Ebenstein, Y.; Avnir, D.; Banin, U. *Chem. Mater.* **2005**, *17*, 258.
(8) Naoi, K.; Ohko, Y.; Tatsuma, T. *J. Am. Chem. Soc.* **2004**, *126*, 3664.
(9) Yang, C.; Kalwei, M.; Schuth, F.; Chao, K. *Appl. Catal., A: Gen.* **2003**, *254*, 289.
(10) Lee, M.; Chae, L.; Lee, K. C. *Nanostruct. Mater.* **1999**, *11*, 195.
(11) Lahiri, D.; Subramanian, V.; Shibata, T.; Wolf, E. E.; Bunker, B. A.; Kamat, P. V. *J. Appl. Phys.* **2003**, *93*, 2575.
(12) Schimpf, S.; Lucas, M.; Mohr, C.; Rodemerck, U.; Bruckne, A.; Radnik, J.; Hofmeister, H.; Claus, P. *Catal. Today* **2002**, *72*, 63.
(13) Hida, Y.; Kozuka, H. *Thin Solid Films* **2005**, *476*, 264.
(14) He, T.; Ma, Y.; Cao, Y.; Yang, W.; Yao, J. *Phys. Chem. Chem. Phys.* **2002**, *4*, 1637.
(15) He, T.; Ma, Y.; Cao, Y.; Yang, W.; Yao, J. *J. Electroanal. Chem.* **2001**, *514*, 129.
(16) Tian, Y.; Tatsuma, T. *Chem. Commun.* **2004**, 1810.
(17) Stepanov, A. L.; Popok, V. N. *Tech. Phys. Lett.* **2003**, *29*, 977.
(18) Fukumi, K.; Chayahara, A.; Kadono, K.; Sakaguchi, T.; Horino, Y. *J. Appl. Phys.* **1994**, *75*, 3075.
(19) Stathatos, E.; Lianos, P.; Falaras, P.; Siokou, A. *Langmuir* **2000**, *16*, 2398.

Scheme 1. Routes to Metal/Semiconductor Nanocomposite Materials

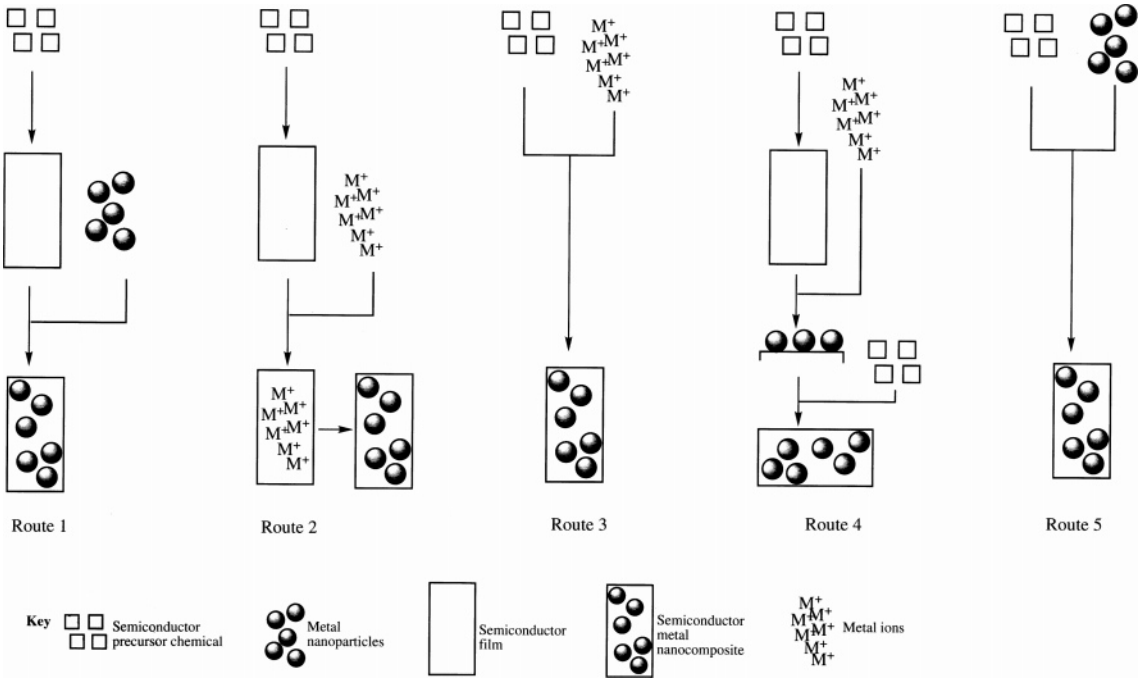

both a semiconductor and nanoparticle precursor,[13,20,21] the related technique of liquid-phase deposition,[22] and multitarget magnetron sputtering deposition.[23] Also, chemical vapor deposition using a separate precursor for each phase falls into this category.[24−26]

Route 4 is the layer-by-layer deposition of metal particles and semiconductor material, for example, laser ablation using alternate metal and semiconductor targets.[27]

In routes 2−4, particles are formed in situ or concurrently with the matrix. There are therefore limits on the type and complexity of nanoparticle that can be incorporated, imposed by the deposition conditions. The use of preformed nanoparticles in route 1 is advantageous because a wider range of nanoparticles can be used. As the semiconductor deposition and nanoparticle formation steps are independent, each can be individually optimized. This strategy seems best for the creation of nanocomposites that include more complex nano shapes and structures.

Here we describe a method for the deposition of nanoparticle/semiconductor composite thin films, which is shown as route 5 in Scheme 1. The method is based on aerosol assisted chemical vapor deposition (AACVD), which uses a liquid−gas aerosol to transport soluble precursors to a heated substrate. The method has traditionally been used when a conventional atmospheric pressure CVD precursor proves involatile or thermally unstable. However, by designing precursors specifically for AACVD, the restrictions of volatility and thermal stability are lifted, and new precursors and films can be investigated. Ionic precursors and metal oxide clusters have been used in aerosol assisted depositions as alternative routes to thin films.[28,29] In this paper we describe AACVD using gold nanoparticle solutions in toluene as precursors. Noble metal colloids may appear to be the antithesis of a CVD precursor, which normally requires volatile molecules, but here we show that preformed gold nanoparticles can be transported in an aerosol generated ultrasonically and can therefore be deposited by AACVD. Nanoparticles can be deposited either alone, yielding nanoparticle films in what is strictly a physical process (no chemical reaction occurs), or together with a conventional CVD precursor, yielding nanocomposite films of gold nanoparticles in a host matrix. Titanium dioxide/gold and tungsten oxide/gold composite films have been produced in this way. Gold nanoparticles were chosen as they are well studied and their synthesis is relatively simple. They were combined with titania and tungsten oxide as these are important technological materials.[13−15] There are two main benefits to this technique over others. First, it is flexible: many preformed nanoparticle solutions could be used, and combined with any chemically compatible conventional precursor, to produce a large range of nanocomposite films. Second, CVD is a widely used industrial technique in fields such as microelectronics and window glass coating, and it has a number of well-known advantages, not least the deposition of adherent, conformal films. Gold/semiconductor nanocomposite films with these qualities can now be easily and inexpensively produced by the method presented here. The method uses preformed particles and a single-step deposition. The Au/TiO_2 films formed in this process have unique optical properties, appearing blue in transmitted light and red to reflected light. Furthermore, the

(20) Yang, Y.; Shi, J.; Huang, W.; Dai, S.; Wang, L. *J. Mater. Sci.* **2003**, *38*, 1243.
(21) Epifani, M.; Giannini, C.; Tapfer, L.; Vasanelli, L. *J. Am. Ceram. Soc.* **2000**, *83*, 2385.
(22) Deki, S.; Ko, H. Y. Y.; Fujita, T.; Akamatsu, K.; Mizuhata, M.; Kajinami, A. *Eur. Phys. J. D* **2001**, *16*, 325.
(23) Qian, W.; Lin, L.; Deng, Y. L.; Xia, Z. J.; Zou, Y. H.; Wong, G. K. L. *J. Appl. Phys.* **2000**, *87*, 1.
(24) Vepfek, S.; Reiprich, S. *Thin Solid Films* **1995**, *268*, 64.
(25) Flahaut, E.; Agnoli, F.; Sloan, J.; O'Connor, C.; Green, M. L. H. *Chem. Mater.* **2002**, *14*, 2553.
(26) Li, D.; Choi, C. J.; Kim, B. K.; Zhang, Z. D. *J. Magn. Magn. Mater.* **2004**, *277*, 64.
(27) Wang, W.; Qu, L.; Yang, G.; Chen, Z. *Appl. Surf. Sci.* **2003**, *218*, 24.
(28) Cross, W. B.; Parkin, I. P.; O'Neill, S. A.; Williams, D. A.; Mahon, M. F.; Molloy, K. C. *Chem. Mater.* **2003**, *15*, 2786.
(29) Binions, R.; Carmalt, C. J.; Parkin, I. P. *Thin Solid Films* **2004**, *469−470*, 416.

Table 1. Parameters Used To Deposit Nanoparticles and Nanocomposite Thin Films on Glass Using Aerosol Assisted CVD[a]

film no.	vol of Au colloid used/mL	conventional precursor, amt	molar ratio Au:precursor	solvent, amt	N_2 flow rate/L min^{-1}
1	5.0	none		toluene, 20 mL	1.0
2	5.0	$W(OPh)_6$, 1 mmol	2:1	toluene, 20 mL	1.0
3	0	$Ti(O^iPr)_4$, 1 mmol		toluene, 50 mL	2.0
4	1.0	$Ti(OiPr)_4$, 1 mmol	1:2	toluene, 50 mL	2.0
5	2.0	$Ti(OiPr)_4$, 1 mmol	1:1	toluene, 50 mL	2.0
6	4.0	$Ti(OiPr)_4$, 1 mmol	2:1	toluene, 50 mL	2.0

[a] All depositions were carried out at 450 °C.

high reflectance demonstrated by these films around 1100 nm means they have great potential for solar control applications.

Experimental Section

Precursor Synthesis. All chemicals were purchased from Aldrich Chemical Co. and used as received without further purification. Gold colloids were synthesized in toluene using the Brust two-phase chemical reduction method.[30] $HAuCl_4 \cdot 3H_2O$ (99%, 0.17 g) was dissolved in deionized water (15 mL). Tetraoctylammonium bromide (TOAB) (99%, 1.04 g) was dissolved in toluene (40 mL), and the two solutions stirred together. A solution of $NaBH_4$ (0.19 g) in deionized water (25 mL) was added dropwise with rapid stirring over a 30 min period, yielding a dark red organic layer. This was separated, washed with portions of dilute aqueous H_2SO_4 and water, dried over Na_2SO_4, and diluted to 100 mL volume with toluene, yielding a dark red solution. The concentration of gold was 4.3 mmol of atoms L^{-1}, 0.85 g L^{-1}. To avoid contamination of films deposited from these solutions, thiol capping groups were not used. As a result, the colloids degraded over time, changing from deep red on synthesis to pale purple or colorless within three weeks when stored at 4 °C. To minimize the effect of colloid degradation on the resulting films, all depositions were carried out using colloids made on the same day. Tungsten phenoxide was synthesized as we have previously described, through the reaction of WCl_6 with phenol in toluene.[28] [$Ti(O^iPr)_4$] (97%) was purchased from Aldrich and used as supplied.

Aerosol Assisted CVD. Depositions were carried out in a cold-wall horizontal-bed CVD reactor. A substrate and top plate were used, both of SiO_2 barrier glass of dimensions 145 × 45 × 5 mm supplied by Pilkington Plc. Deposition was carried out on the SiO_2 barrier layer to prevent migration of ions into the film from the glass bulk. The substrate rested on a carbon heating block powered by a Whatmann cartridge heater; the temperature was monitored by Pt−Rh thermocouples. A top plate was positioned parallel to the substrate and 8 mm above it, and the whole assembly was contained within a quartz tube. An aerosol was generated from the precursor solution in a glass flask using a Pifco ultrasonic humidifier with an operating frequency of 40 kHz. The aerosol was directed to the reactor by nitrogen gas through PTFE and glass tubing, entering the reactor between the top plate and substrate; reactor waste left via an exhaust port. The gas flow was continued until all the precursor mix had passed through the reactor, typically taking 20−30 min depending on the gas flow rate. Films were cooled in situ under a flow of nitrogen gas, and subsequently were handled and stored in air.

Analysis. X-ray photoelectron spectroscopy (XPS) measurements were carried out on a VG ESCALAB 220i XL instrument using monochromatic Al Kα radiation. Binding energies were referenced to surface elemental carbon 1s peak with binding energy 284.6 eV. UV/vis spectra were obtained using a Thermo Helios-α spectrometer. Where a solution spectra was taken, quartz cuvettes with a path length of 1 cm were used. Scanning electron microscopy (SEM) and energy dispersive X-ray (EDX) analysis were carried out using a JEOL 6301F instrument using voltages between 6 and 15 kV, at 8 μA. Before SEM analysis, samples were sputter coated with gold using an Edwards S150B sputter coater, operating at 1.5 kV and 20 mA. Transmission electron microscopy (TEM) was performed on gold nanoparticle solutions, and was carried out on a JEOL JEM 100CX II. TEM samples were prepared by evaporating a single drop of the sample onto a conducting copper mesh. Powder X-ray diffraction (XRD) patterns were obtained on a Bruker AXS D8 instrument using Cu Kα radiation. To record diffraction peaks from the thin films, a fixed incidence angle of 5° was used. Diffraction patterns were recorded with an area detector. Color data, reflectance/transmittance spectra, and haze measurements were recorded on a HunterLab UltraScan Pro instrument. Color analysis was performed at 2° viewing angle using D65 artificial daylight, which was also used for haze measurements.

Results

The initial stock gold nanoparticle solutions used were deep red in color. Their UV/vis spectra showed a plasmon resonance peak with a maximum at 533 nm. TEM revealed a mean diameter of 10 nm and narrow particle size distribution.

Depositions of thin films on glass were carried out as shown in Table 1. Three types of film were deposited: gold nanoparticle films from the gold nanoparticle solution alone (film 1), WO_3/Au composite films from [$W(OPh)_6$] and gold nanoparticle solution (film 2), and TiO_2/Au composite films from [$Ti(O^iPr)_4$] and gold nanoparticle solution (films 4, 5, and 6). A series of titania films with different concentrations of gold nanoparticles were deposited. The flow rates and volumes of solvent used were selected to give the most extensive deposition over the substrate.

Gold Nanoparticle Films. The deposition of gold nanoparticles from gold colloid solutions occurred on both the substrate and top plate, which is the glass plate that rests 8 mm above the surface of the substrate. Films deposited on the substrate were used in the analysis described below. Gold nanoparticle films appeared red to transmitted light and yellow to reflected light. The films were stored and handled in air with no apparent degradation; however, the films were nonadherent and could be easily removed by slight mechanical abrasion. The glass could be wiped completely clean with a tissue, indicating that the gold particles were weakly adsorbed on the glass surface, rather than strongly bound to it or absorbed within it. UV/visible spectroscopy revealed the characteristic gold plasmon resonance peak, with a maximum at 538 nm (Figure 1). This was very similar in position and shape to the plasmon peak observed in the initial gold nanoparticle solution, which had a maximum at 533 nm, suggesting that the mean size and shape of the particles are roughly similar to those of the precursor colloid. Au 4f 7/2 and 5/2 peaks at binding energies of 87.5 and 83.7 eV, respectively, corresponding to metallic gold, were observed by XPS.[41] SEM confirmed the presence of individual nanoparticles

(30) Brust, M.; Walker, M.; Bethell, D.; Schiffrin, D. J.; Whyman, R. *J. Chem. Soc., Chem. Commun.* **1994**, 801.

(31) O'Neill, S. A.; Clark, R. J. H.; Parkin, I. P.; Elliott, N.; Mills, A. *Chem. Mater.* **2003**, *15*, 46.

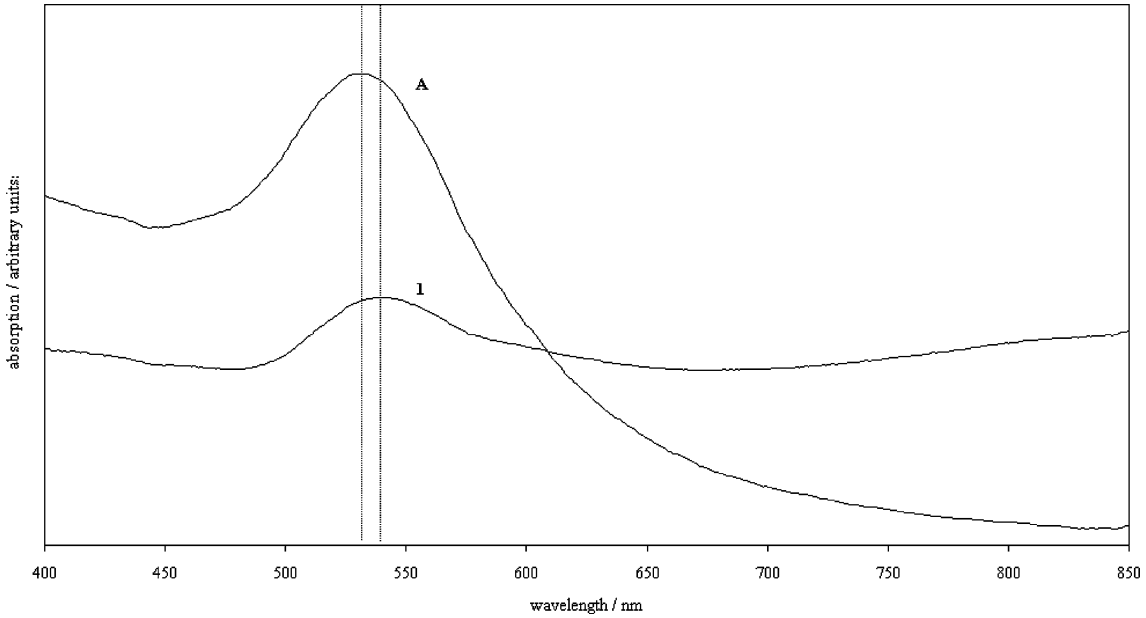

Figure 1. UV/visible spectra of gold nanoparticles in toluene (A) and gold nanoparticle film on glass (1) deposited by AACVD, both showing a plasmon resonance peak.

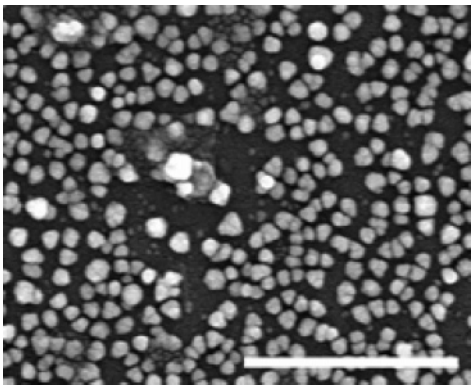

Figure 2. SEM image of gold nanoparticle film on glass (film 1, Table 1), produced by aerosol assisted CVD. The scale bar measures 1 μm.

on the surface of the film (Figure 2). The particles appear randomly distributed, roughly spherical, and around 50 nm in diameter. Some particles seem to be agglomerates of two, three, or more smaller particles. In other places, two or three particles can be observed in close proximity but not conjoined. Bare glass is visible between the particles, showing that less than one monolayer has been deposited. Assuming the particles to be spherical, this places the maximum film thickness at 50−100 nm, the diameter of a single particle.

The apparent increase in particle size could be due to agglomeration of particles, either in the gas phase or on the substrate surface. In either case, it is significant that the deposition yields a nanoparticulate film rather than a continuous metal film or highly agglomerated particles, which might be expected due to the associated energetically favorable reduction of surface area and the relatively high temperature of deposition. No nitrogen or bromine peaks were observed in the XPS spectrum, indicating that atoms from the tetraoctylammonium bromide used in the synthesis, which prevented particle agglomeration in solution, are no longer present. This suggests that the gold particle mobility on the surface is low, even at the deposition temperature, preventing aggregation and continuous film formation.

Titania/Gold Nanocomposite Films. Titania films were deposited with 1, 2, and 4 mL of 4.3 mM gold nanoparticle solution (Table 1). The molar ratios of Ti:Au used in each experiment were approximately 1:2, 1:1, and 2:1, respectively. All films were deposited at a substrate temperature of 450 °C. The films differed in thickness throughout the substrate, but samples taken for analysis were approximately 300 nm in thickness, determined by the pattern of interference fringes. Undoped titania films produced by CVD are typically colorless or pale yellow.[31] Titania/gold composite films appeared pale blue to transmitted light, with the intensity of the blue color increasing with increasing gold nanoparticle content. All titania composite films were strongly adherent to the glass, such that they could not be removed by vigorous rubbing with tissue paper and were undamaged in routine handling. Application of pressure with a stainless steel stylus caused small portions of the film to chip away. Optical haze, being the percentage of D65 artificial daylight scattered by the films, was measured to be 0.40%, 0.55%, and 0.75% for films 4, 5, and 6, respectively. All these values are comparable to commercial window coatings, which typically have below 0.5% optical haze.

UV/vis spectroscopy of the TiO_2/Au composite films showed absorption peaks in the region of 580 nm which are assigned

(32) Link, S.; El-Sayed, M. A. In *Semiconductor and Metal Nanocrystals*; Klimnov, V. I. Ed.; Marcel Dekker: New York, 2004; p 45.
(33) For more information on the CIELAB color space system refer to http://www.cie.co.at/cie (the Web page of the CIE) or http://www.colourware.co.uk/cpfaq/q3-21.htm.
(34) Dzhurinskii, B. F.; Gati, D.; Sergushin, N. P.; Nefedov, V. I.; Salyn, Y. A. V. *Russ. J. Inorg. Chem.* **1975**, *20*, 2307.
(35) Talbot, L.; Cheng, R. K.; Schefer, R. W.; Willis, D. R. *J. Fluid Mech.* **1980**, *101*, 737.
(36) Palgrave, R. G.; Parkin, I. P. *J. Mater. Chem.* **2004**, *14*, 2864.
(37) Kielbassa, S.; Kinne, M.; Behm, R. J. *J. Phys. Chem. B* **2004**, *108*, 19184.
(38) Klar, T.; Perner, M.; Grosse, S.; von Plessen, G.; Spirkl, W.; Feldmann, J. *Phys. Rev. Lett.* **1998**, *80*, 4249.
(39) Barreras, F.; Amaveda, H.; Lozano, A. *Exp. Fluids* **2002**, *33*, 405.
(40) Choy, K. L. *Prog. Mater. Sci.* **2003**, *48*, 57.
(41) Brooks, A. R.; Clayton, C. R.; Doss, K.; Lu, Y. C. *J. Electrochem. Soc.* **1986**, 2459.

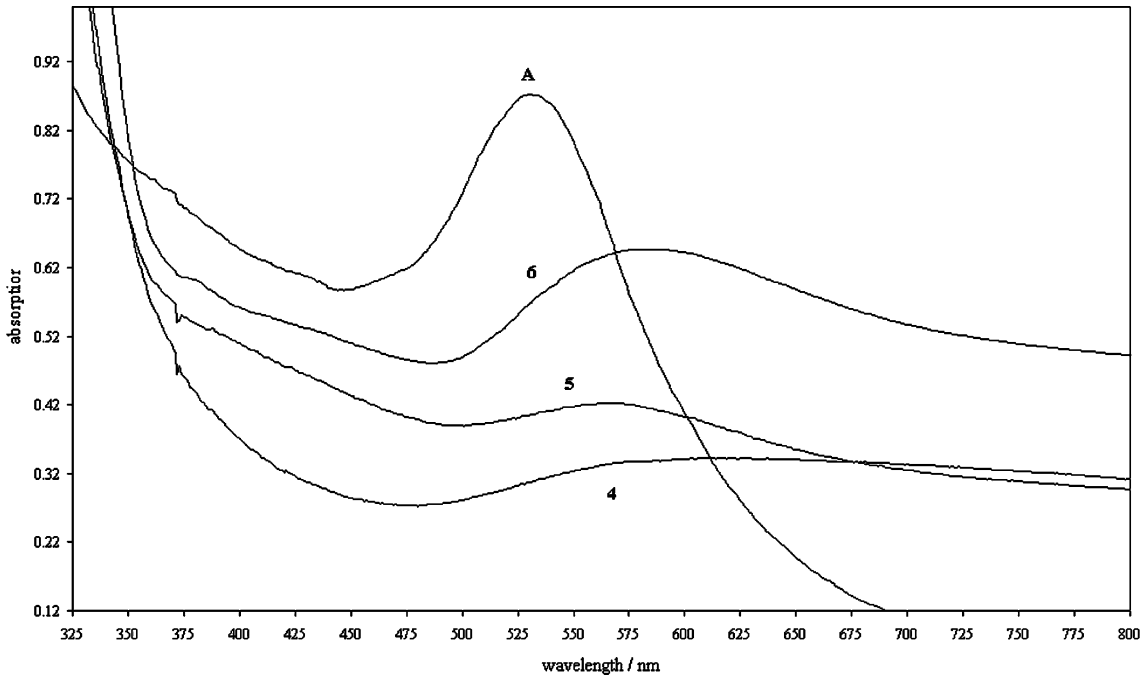

Figure 3. UV/visible spectra of (A) gold colloid suspended in toluene used as a precursor solution and (4, 5, 6) TiO_2/Au composite films of increasing gold content (see Table 1) deposited on glass using aerosol assisted CVD.

to the red-shifted and broadened plasmon resonance of gold nanoparticles (Figure 3). The gold nanoparticles could not be removed from the TiO_2/Au composite film by immersion in common organic solvents or water, or by abrasion, as indicated by the persistence of the plasmon absorption peak after these treatments. Indeed, the gold particles could not be removed by any physical method that did not also remove the titania film, showing that the nanoparticles are either strongly bound to the film or firmly contained within it. The red shift of the plasmon absorption peak has been observed in similar nanocomposites,[20] and can be accounted for in a number of ways. As the particles are incorporated in titania, a matrix of high dielectric constant, light will be absorbed at a longer wavelength. Red shifting of the plasmon peak also occurs with an increase in particle size,[32] or a reduction in particle spacing.[4] All three factors probably contribute to the change in position of the plasmon peak in these nanocomposite films, and are difficult to deconvolute. The latter two factors also cause broadening of the peak,[4,32] and in addition, a wider size and shape distribution is also expected to cause peak broadening.

The intensity of the plasmon absorption in the TiO_2/Au films increased with increasing gold concentration. The reflectance/transmission spectrum of the highest concentration composite film was measured in the visible and IR regions (Figure 4). The plasmon peak can be seen as a local minimum in the transmission spectrum at 580 nm, and the titania band edge is present at 390 nm. Other than these two features, the transmission spectrum is qualitatively that of the float glass substrate. The reflectance spectrum shows a highly unusual broad peak in the red and near-infrared regions with a maximum at 805 nm, where 35% of incident light is reflected. This feature is not characteristic of titania or glass, so it must arise from the gold particles. Indeed, related peaks have been observed in matrixes of Au@SiO_2 core−shell nanoparticles, where the position and intensity of the reflection maximum was found to be strongly dependent on the particle spacing.[4] It is also predicted by the Maxwell−Garnett model, which can be used to predict the optical properties of dense assemblies of interacting nanoparticles.[4] The optical spectra will be considered in more detail below.

One of the most immediately striking properties of the titania−gold composite films is their color. The color was quantified using the CIELAB color coordinates, which are used to express perceived color and are an industry standard (Figure 5).[33] Two parameters, a^* and b^*, define the color: positive a^* values correspond to red, negative a^* values to green. Positive b^* values correspond to yellow, negative b^* values to blue. Figure 5 shows the color of the high concentration TiO_2/Au composite thin film to both transmitted and reflected light. Transmitted light is blue-green, while reflected light is red, which is consistent with the visible spectra (Figures 3 and 4). For comparison, data are given for 5 mm thick sheets of transition metal doped (body tinted) glass. Untreated glass has close to no color (a^* and b^* are close to zero), while Fe and Nd doped glasses are strongly colored. Significantly, the intensity of transmitted color imparted by the composite film is comparable to commercial body tinted glass, despite the film being around 4 orders of magnitude thinner; the extinction coefficients of gold particles are known to be greater than typical organic or transition metal dyes.[32] These films might therefore be used as colored coatings with a coloration of similar magnitude to that of traditional body tinted glass. Furthermore, the near symmetric opposite coloration of these films in reflected and transmitted light is unusual. This type of dichromism has been seen in bulk materials that contain a dispersion of metal nanoparticles. An example is the Lycurgus Cup, a Roman artifact made of glass containing embedded Au, Ag, and Cu nanoparticles.[42]

SEM imaging of the TiO_2/Au films showed bright particles on a darker textured background, interpreted as gold nanopar-

(42) Barber, D. J.; Freestone, I. C. *Archaeometry* **1990**, *32*, 33.

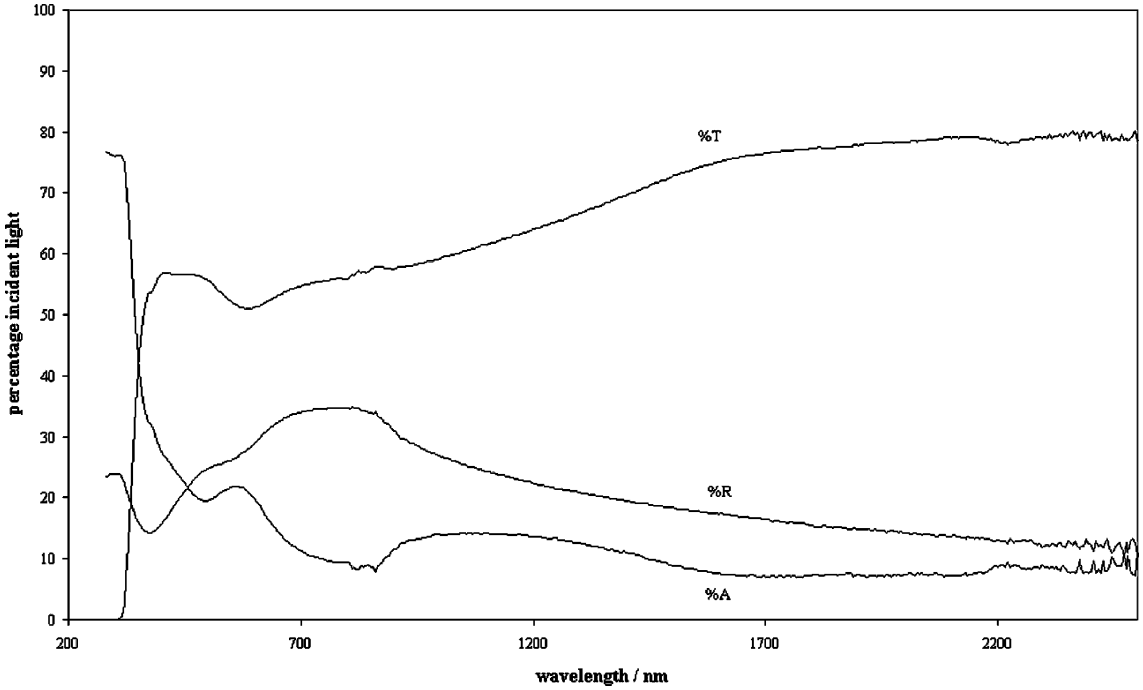

Figure 4. Reflectance (%R), transmission (%T), and absorption (%A) spectra of titanium dioxide/gold nanocomposite film (6) on glass in visible and IR regions.

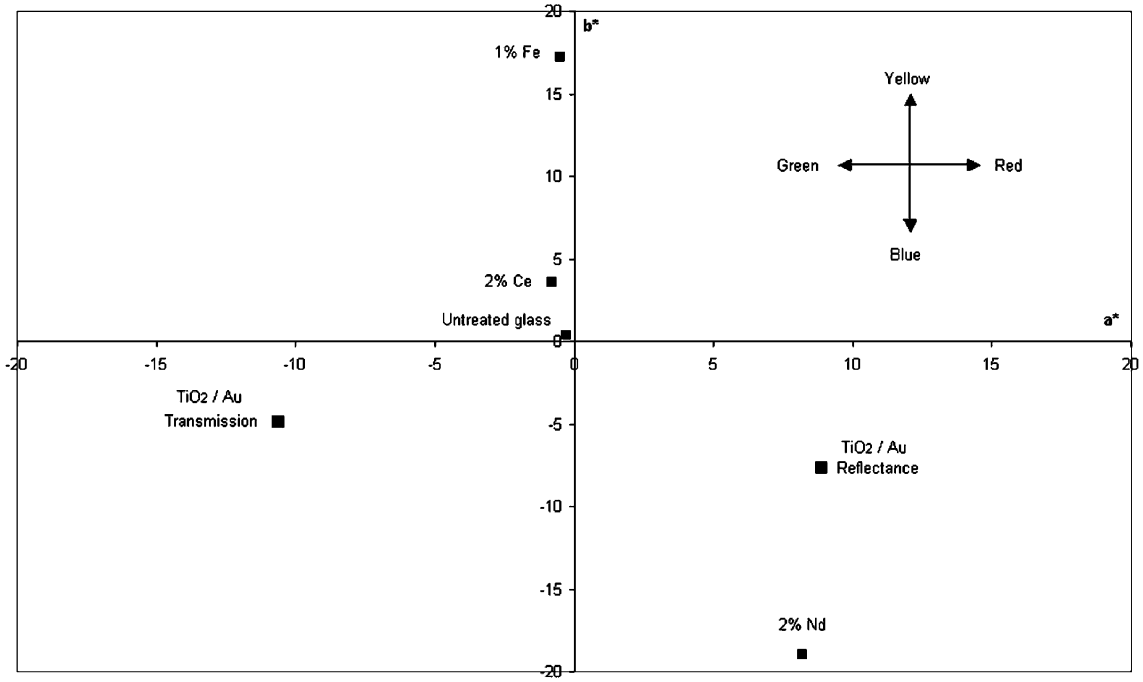

Figure 5. Color space representation of the color of light reflected and transmitted by titanium dioxide/gold nanocomposite film (6). For comparison, the color of light transmitted through 5 mm of untreated glass and 5 mm of glass treated with various concentrations of transition metal ions, known as body tinted glass. The *a** axis quantifies red and green, and the *b** axis quantifies yellow and blue.

ticles embedded in a titania matrix. The particles appeared randomly distributed and oriented. Some particles had formed larger agglomerations, but the majority were less than 100 nm in diameter. Figure 6 shows SEM images of titania films with different concentrations of gold particles. No particles could be seen in the film of lowest concentration, but in films with higher concentrations particles were visible. The particle number density increases with increasing precursor Au concentration, but the particle size distribution is roughly constant. XRD detected crystalline gold in the composite films (Figure 7); peaks at 2θ values of 38.2° and 44.5° (Cu Kα radiation) arise from the (111) and (200) planes in the Au cubic lattice.[20] The intensity of those peaks increased with increasing gold incorporation, although the width remained approximately constant. The Scherrer equation was used to estimate the gold crystallite diameter using the (111) peak. In the two films of highest gold concentration, this was found to be 10 nm. This diameter is much smaller than the particles observed by SEM, suggesting that each particle is composed of several crystals, most probably several of the original precursor nanoparticles. It appears,

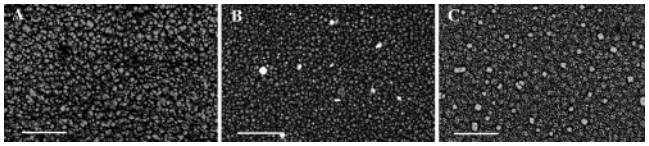

Figure 6. SEM images of titania/gold nanocomposite films. Gold particles are visible as bright spots against a darker background, due to their higher electron density. Images A, B, and C are taken from films 4, 5, and 6, respectively (Table 1). A greater number of particles can be seen in films made from higher concentrations of gold colloid precursor.

therefore, that there is some degree of particle agglomeration at some point during the deposition, either in the gas phase or on the surface of the substrate. However, this agglomeration does not change the intrinsic crystallite size of the Au particles—which are unchanged from the initial Au colloid solution. No TiO_2 peaks were observed in the X-ray diffraction pattern, indicating that the deposited titania matrix had low crystallinity. XPS was performed on the titania film with the highest concentration of gold. This confirmed the presence of gold and titanium in the film; a single gold environment was observed with Au 4f 7/2 and 5/2 peaks at binding energies of 83.4 and 87.2 eV respectively, corresponding to Au metal. This shows that the nanoparticles do not undergo a chemical reaction in the CVD process, for example oxidation, and they remain metallic. Ti 2p 1/2 and 3/2 binding energies were observed at 458.8 and 464.9 eV, corresponding to Ti^{4+} ions in TiO_2.[34] Quantification using peak areas gave a gold-to-titania atomic ratio of around 1:100 at the surface. In the bulk, the Au:Ti ratio rose to 1:25, as determined by EDX. Both these values are much lower than the concentration in the original precursor solution (Table 1), and this may be due to the deposition of Au particles on the cold walls and top plate of the CVD apparatus, a result of the thermophoretic effect.[35]

The titania/gold composite films were annealed in air at 550 °C for 20 min periods. Annealed films appeared a lighter shade of blue than before annealing, and correspondingly the UV/vis absorption maximum shifted to longer wavelengths, became broader, and increased in intensity, as shown in Figure 8. The greatest change to the optical spectra was seen after 20 min of annealing, and no further change was observed after 80 min (Figure 8). These specific changes to the plasmon peak are discussed in the following section. A similar shift has been observed in composite films of gold and barium titanate.[20] In the data presented here, the breadth of the peaks was calculated using the peak half-width at three-fourths maximum on the low-energy (red) side of the peak.

XRD (Figure 9) showed that the gold peaks became slightly narrower on annealing: the full width at half-maximum (fwhm) of the more intense (111) peak fell by 0.1° for the two films with highest concentrations of gold after 20 min at 550 °C, indicating a small increase in crystallite size. In contrast, the titania cystallinity increased markedly. Peaks corresponding to anatase phase titania appeared after annealing at 2θ values of 25.9°, 48.7°, and 54.6°, as shown in Figure 9. The higher the concentration of gold in the film, the more intense these emergent titania peaks were, although the peak width was similar. The gold particles might act as nucleation sites for titania crystal growth; hence films with a higher number of gold particles show larger amounts of crystalline titania.

Tungsten Oxide/Gold Nanocomposite Films. To assess whether the method could be extended to other matrix materials, depositions using gold colloid and tungsten hexaphenoxide were carried out (Table 1). Tungsten oxide/gold composite films were dark blue on deposition, due to the presence of reduced tungsten states in a WO_{3-x} stoichiometry. Dark blue substoichiometric tungsten oxide has been previously deposited by AACVD, and is not due to the presence of nanoparticles.[28,36] The films were adherent and continuous, and could not be removed from the glass by vigorous rubbing with a tissue. Application of pressure with a metal stylus caused small portions of the film to chip away. No gold plasmon peak was directly observed in the UV/

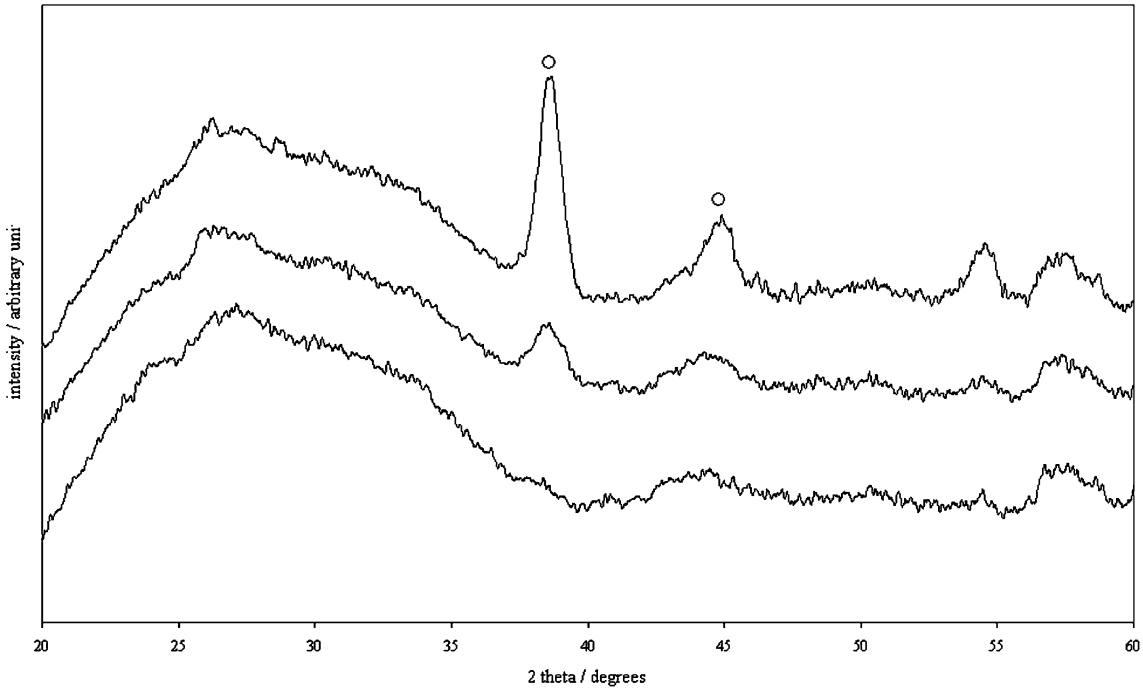

Figure 7. Glancing-angle powder XRD patterns of TiO_2/Au composite films, showing cubic gold peaks (○). From bottom, films 4, 5, and 6 (Table 1). The intensity of the gold peaks increases with increasing gold concentration.

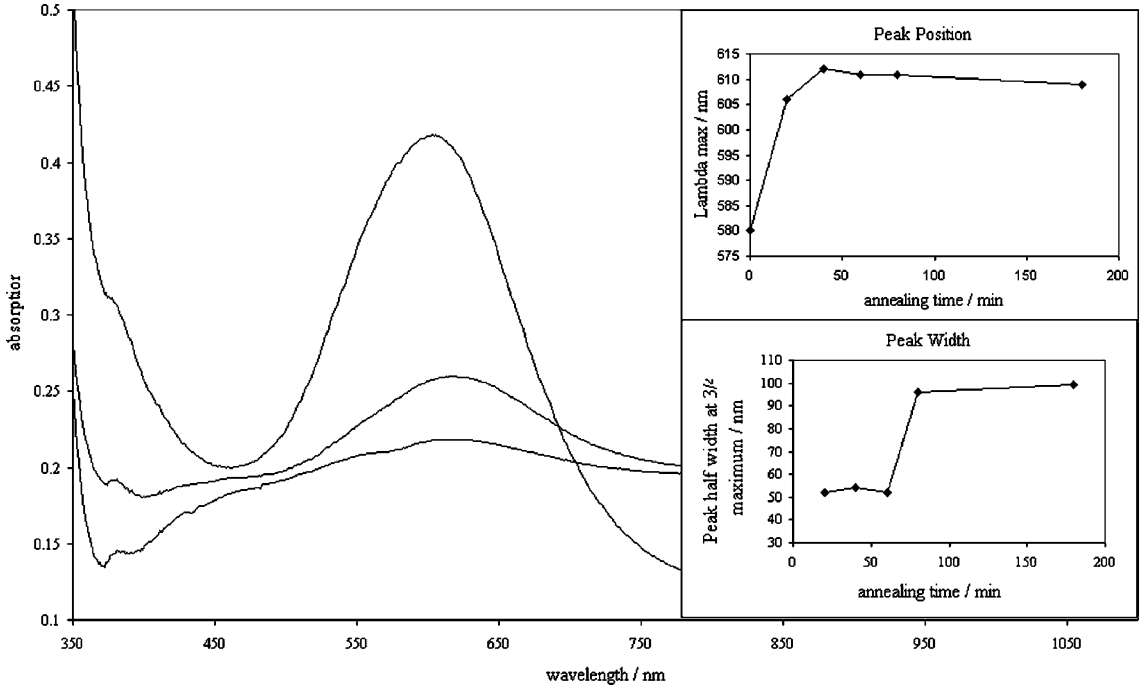

Figure 8. Left: UV/visible spectra of TiO_2/Au composite films after annealing at 550 °C for 20 min. From bottom, films 4, 5, and 6 (Table 1). The intensity of the plasmon peak increases with increasing gold concentration. Right: Changes in optical absorption of film 6 (high Au concentration) on extended annealing at 550 °C. The plasmon peak shifts to higher wavelengths and becomes broader on annealing.

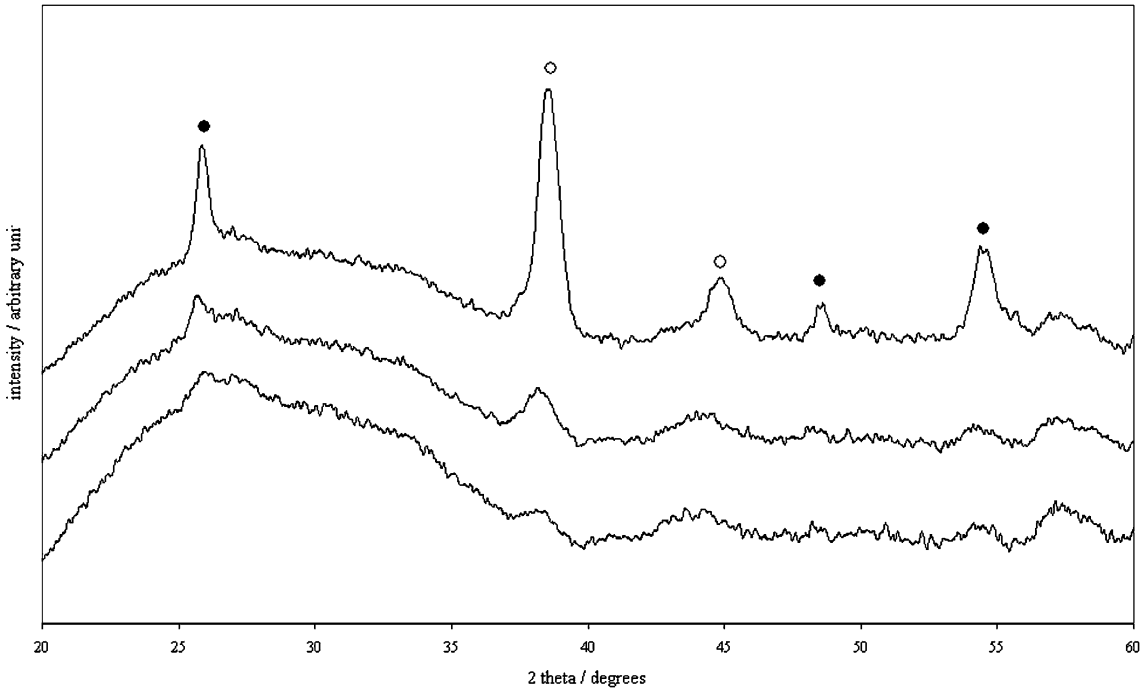

Figure 9. Glancing-angle powder XRD patterns of TiO_2/Au composite films after annealing at 550 °C for 20 min. Cubic gold peaks (○) and anatase TiO_2 peaks (●) are present. From bottom, films 4, 5, and 6 (Table 1). The films with higher concentrations of gold show more intense anatase peaks, showing that gold particles promote crystallization of the host matrix.

vis spectrum, although it was probably masked by the strong visible absorption of the tungsten oxide. An XRD pattern, shown in Figure 10, showed cubic gold peaks at 2θ values of 38.8° and 45.1° assigned to (111) and (200) planes. Two strong peaks at 2θ values of 23.9° and 48.5° are assigned to the (020) and (040) reflections of monoclinic WO_3, with strong preferred orientation in the (020) direction, as previously observed in WO_3 films deposited from $[W(OPh)_6]$.[28] The presence of crystalline gold XRD peaks is strong evidence that gold nanoparticles are present in the film as deposited despite the lack of a visible plasmon peak. In addition, SEM imaging (Figure 11) shows randomly distributed particles embedded in the tungsten oxide matrix.

The tungsten oxide/gold films were annealed at 450 °C for 20 min. On annealing, the films became pale yellow, corresponding to fully oxidized WO_3. After annealing UV/vis spectroscopy showed a plasmon peak at 604 nm. As with the titania composite films, no method could be found to remove

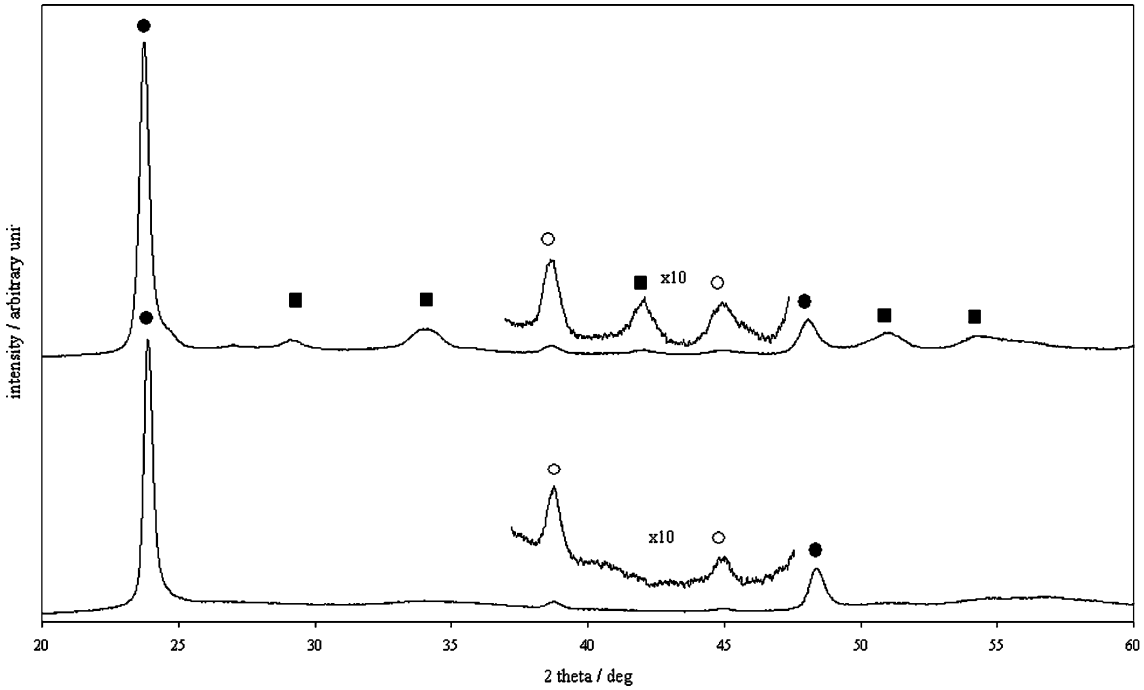

Figure 10. Glancing-angle powder XRD patterns of WO_3/Au composite films before (bottom) and after (top) annealing at 450 °C for 20 min. Before annealing, cubic gold (○) and the (020) and (040) peaks of monoclinic WO_3 (●) are present, showing strong preferred orientation of the semiconductor film. After annealing, peaks from other monoclinic WO_3 planes are present (■), indicating some randomization of the orientation of crystals in the film.

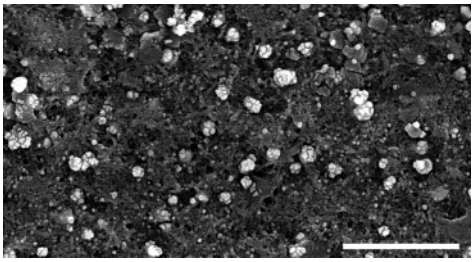

Figure 11. SEM image of tungsten oxide/gold nanocomposite film, 2 (Table 1). The scale bar measures 1 μm. Gold particles are visible as bright spots against a darker background, due to their higher electron density.

the nanoparticles without also removing the tungsten oxide coating. XRD showed the emergence of monoclinic tungsten oxide peaks absent in the preannealed film, although the intensity was lower than the (020) and (040) peaks. No change in the tungsten oxide (020) and (040) peaks was observed. This can be interpreted as the partial randomization of the crystallite orientation after annealing, although strong preferred orientation remains.[28] As in the titania composite films, the gold peaks did not significantly change on annealing. XPS confirmed the presence of tungsten oxide and gold in the annealed films, showing Au 4f peaks at 84.3 and 88.0 eV. These binding energies were slightly higher than seen in the TiO_2/Au composite, although within the range expected for Au metal nanoparticles.[37] Tungsten was observed in a single environment with W 4f peaks at 35.9 and 38.1 eV, indicating W^{6+} ions in WO_3. The lack of W^{4+} and W^{5+} environments confirms the full oxidation of the tungsten oxide to stoichiometric WO_3 by the annealing process.

Discussion

Nanoparticles in Chemical Vapor Deposition. To the best of our knowledge, in current CVD processes that deposit nanoparticles or nanostructures in general (e.g., rods, wires, tubes), the nanoobjects form in the CVD reactor itself from the reaction of one or more precursors. Examples include the works of Verprek et al.,[24] Flahaut et al.,[25] Choi et al.,[26] and many others. In all these cases, the deposition conditions must be controlled to ensure the correct size and shape of nanoobject is formed. The aerosol assisted method presented here shows that CVD using preformed nanoparticles as precursors is possible. As such, the nanoparticle synthesis is distinct from the deposition step, so that deposition parameters do not need to be tailored to accommodate nanoparticle formation. Rather, parameters can be chosen to suit the conventional precursor and substrate, although the transport of nanoparticles to the substrate must still be considered. In addition, it is expected that nanoparticles of complex compositions might be used, such as core−shell particles or alloys, which might be difficult to produce in situ in a CVD reactor.

The size of the toluene aerosol droplets produced by the ultrasonic humidifier can be estimated as 20 μm using Lang's method, which relates the vibration frequency (in this case 40 kHz), surface tension, and density of the liquid to aerosol droplet size.[39,40] The density and surface tension of pure toluene were used for this calculation. Assuming that the concentration of nanoparticles in the aerosol droplets is the same as in the bulk precursor solution, and that the particles are 10 nm spheres, as shown by TEM, the number of gold nanoparticles in a single aerosol droplet can be calculated. In the highest concentration solution, used to deposit gold nanoparticle films and tungsten oxide/gold nanocomposite films (films 1 and 2), there are around 1.4×10^4 nanoparticles per droplet. Titania/gold composite films (4, 5, and 6) were deposited with concentrations of 1.2×10^4, 5.8×10^3, and 2.9×10^3 particles per droplet, respectively. The gold particles observed in the composite and nanoparticle films are larger than those in the precursor solution, indicating

that agglomeration has taken place. However, it is clear that it is not the entire contents of an aerosol droplet that agglomerates.

The behavior of nanoparticles in the CVD reactor differs from that of a conventional molecular precursor due to the relatively large size of the nanoparticle. Gas-phase particles are subject to a thermophoretic force when exposed to a temperature gradient.[35] This force is directed away from the hot surface, so particles act as if repelled from a hot surface and attracted toward a cold surface. This is usually of benefit in CVD as it prevents particles (formed by gas-phase reaction of precursors or otherwise present) from being incorporated into the growing film. Since the flow of gas in the reactor is laminar rather than turbulent, thermophoresis is usually the dominant force determining the deposition location of particles. It is therefore unsurprising that when deposited alone, without an additional precursor, the majority of gold nanoparticles are found on the top plate. However, when deposited with an additional precursor, gold particles are present throughout the substrate coating, indicating that the presence of an additional precursor somehow overcomes the thermophoretic effect. One possibility is that gas-phase reaction of the precursor on the surface of the gold nanoparticles produces coated gold particles, which are less affected by the asymmetric bombardment of gas molecules than smaller, uncoated particles. They can therefore find their way to the substrate more easily. Nonetheless, the reduction in Au:Ti atomic ratio from around 2:1 to around 1:25 in film 6 (as quantified by EDX analysis) indicates that a large proportion of the gold is lost during deposition. This indicates that the majority of gold particles are deposited on the cold walls of the reactor and the top plate, or pass from the reactor in the exhaust, rather than deposit on the substrate.

Film Color and Optical Properties. The color and optical spectra are perhaps the most interesting features of the composite films produced in this study, and these characteristics are dominated by the plasmon resonance of the gold nanoparticles incorporated within the films. Three observations are important here: the red shifting of the plasmon peak on deposition, the further red shifting on annealing of the films, and the reflection peak in the red and near-IR regions. Mie theory is frequently used to model the plasmon peak in gold and other metallic nanoparticles. Mie theory is applicable to low particle concentrations, including isolated single nanoparticles,[38] but breaks down in very dense colloids, where significant dipole interaction between the particles occurs.[5,6] In this intermediate regime, between nanoparticulate and bulk phases, the Maxwell−Garnett (MG) model has been used to predict the plasmon resonance.[5] We have considered which model best fits the observations cited here, and whether the particles in the films behave in isolation or interact.

Mulvaney et al. studied films of Au@SiO_2 core−shell particles on glass, the gold cores of which showed dipole interaction.[4] In their work, the MG model was used to successfully predict the optical properties of dense arrays of gold particles that were kept physically separate by their surrounding layers of silica. This structure bears a resemblance to the nanocomposite materials produced in this work, where gold particles are also separated by a dielectric material. This is especially true if, as discussed above, the gold particles acquire a shell of TiO_2 during the CVD process. The optical spectra for both sets of films show similar features. The reflection spectra of the Au@SiO_2 core−shell films showed peaks in reflectivity in the red and near-IR regions, which were dependent on particle separation. Mulvaney et al. successfully explained this using the MG model of dipole interaction between the particles.[4] That this peak also appears in the reflectance spectrum of the titania/gold nanocomposite films is strong evidence that the gold particles therein are close enough to interact. As mentioned above, the gold particles might acquire a thin titania coating during the deposition process. If so, then this titania layer would prevent gold particles fusing while allowing them to come close enough to interact as described by the MG model.

In addition, the MG model predicts red shifting of the plasmon peak with reduced particle separation, which might explain the change in plasmon peak on deposition (Figure 3). However, Mie theory provides an alternative explanation, that the particles may fuse, creating larger particles, which also show a red-shifted plasmon peak. Of course it may be that case that both mechanisms are at work, and both contribute to the plasmon red shift. Nonetheless, the further red shift on annealing is probably better explained by the MG model. In the absence of any gold ions in the sample (as shown by XPS), this must be caused by either an agglomeration of particles or a reduction in separation of dipole interacting particles. Annealing is known to increase film density by eliminating pores and voids, and thus would be expected to reduce particle separation. The MG model can thus explain the red shifting of the plasmon peak on annealing of the films. The absence of any further red shift after 80 min of annealing represents the elimination of all the voids and the limit of the mobility of the particles within the film.

Potential Applications. A wide range of applications has been suggested for semiconductor/metal nanocomposites in general, as outlined in the Introduction. In addition, several other possibilities present themselves. The reflection properties of the titania/gold films may lend themselves to heat mirror applications, since they reflect infrared light and transmit visible light. Heat mirrors are used in solar control applications. In this case the higher reflectivity in the near-IR would mean that a window incorporating these particles would reflect away much of the heat portion of solar radiation (which is most intense between ca. 800 and 1500 nm). This would enable a reduction in solar gain and a reduction in air conditioning costs. The optical clarity of the films makes them suitable for use as window coatings where tinted glass is required. This would be a valuable alternative to body tinting—the current practice of coloring the whole pane of glass—as it is an expensive process to implement on a glass float line. A coating that gave the same intensity in color, and whose color could be varied by a simple change in precursor concentration, may make tinted glass much less expensive to produce. However, we believe that the main application of this technique lies in the variety of films that can be produced by varying the precursors and nanoparticles used. One obstacle that must be overcome is the relatively low efficiency of incorporation of nanoparticles into the films.

Conclusion

Metallic gold nanoparticles can be deposited as thin films with little change in their size or shape, and without chemical reaction, under AACVD conditions. They can also be deposited in conjunction with conventional CVD precursors, resulting in the formation of continuous, durable nanocomposite films

containing randomly distributed nanoparticles, as demonstrated by TiO_2/Au and WO_3/Au depositions. The gold particles cannot be removed from the composite films without also removing the metal oxide coating. The concentration of nanoparticles in the film can be altered simply by changing the concentration of gold colloid in the precursor mix. No reaction takes place between the film and the gold particles, although the gold plasmon resonance peak shifts to longer wavelengths on incorporation, due to a variety of factors including the high refractive indices of the metal oxide films, dipole interaction between particles, and an increase in mean particle size. On annealing, the plasmon peak shifts to higher wavelengths in titania/gold composite films, which is best explained by a reduction in particle separation. The gold particles show cubic Au peaks in the XRD pattern of the film. The presence of gold nanoparticles can enhance the crystallization of titania: films with higher proportions of gold particles showed a greater increase in anatase X-ray diffraction peaks on annealing, compared to films with lower concentrations of gold.

The technique described here could be extended by using a variety of nanoparticles and conventional precursors, and so provide a new and versatile CVD route to nanocomposite films.

JA055563V